The fragmentation of ^{20}Ne at 400 A MeV*

CHENG Jin-Xia(程锦霞)[1] ZHANG Dong-Hai(张东海)[2;1)] YAN Shi-Wei(晏世伟)[1,3]
LI Jun-Sheng(李俊生)[2] WANG Li-Chun(王立春)[1] LI Yan-Jing(李彦晶)[1] N. Yasuda[4]

[1] College of Nuclear Science and Technology, Beijing Normal University, Beijing 100875, China
[2] Institute of Modern Physics, Shanxi Normal University, Linfen 041004, China
[3] Beijing Radiation Center, Beijing 100875, China
[4] Fundamental Technology Center, National Institute of Radiological Sciences 4-9-1 Anagawa, Inage-ku, Chiba 263-8555, Japan

Abstract: The total charge-changing cross sections and partial cross sections for the production of projectile fragments are measured in the interactions of 400 A MeV ^{20}Ne with aluminum, carbon and polyethylene targets sandwiched with CR-39 plastic nuclear track detectors. The measured total charge-changing cross sections are compared with the predictions using the Bradt-Peters semi-empirical formula, and the NUCFRAG2 and PHITS models. It is shown that the measured experimental results are in good agreement with the theoretical model prediction and other experimental results, and it can be clearly seen that the partial cross sections for fragment production show obvious odd-even effects.

Key words: heavy ion, fragmentation, charge-changing cross sections, CR-39

PACS: 25.75.-q, 25.70.Mn, 25.70.Kk **DOI:** 10.1088/1674-1137/36/1/006

1 Introduction

It is important to understand the fragmentation of heavy ions in high-energy nucleus-nucleus interactions for many applications in areas such as astrophysics, radiobiology and radiotherapy [1]. Light-ion beams such as ^{12}C, ^{16}O and ^{20}Ne, with kinetic energies of a few hundred MeV/nucleon offer favorable conditions for the treatment of deep-seated tumors in cancer therapy [2]. Light ions exhibit an excellent physical depth-dose profile (Bragg curve), and in addition a low relative biological effectiveness (RBE) in the plateau of the Bragg curve and an increased RBE in the Bragg peak region. However, nuclear fragmentation affects the dose vs depth profile and must be taken into account in treatment planning. In space, the fragments of heavy ions in galactic cosmic rays can be produced in healthy cells and may have a bad effect on astronaut health. Nuclear fragmentation has been extensively studied both theoretically [3–6] and experimentally [7–13] for many years, but there still remain some discrepancies, not only between experiments and theoretical prediction models [14], but also between the experiments themselves [7, 15]. Therefore, an accurate description of heavy ion fragmentation is necessary in understanding the effect on humans in medicine [16] and in space [17].

In this paper, the total charge-changing cross sections and partial fragment production cross sections of 400 A MeV ^{20}Ne collisions with C, Al and CH_2 targets sandwiched with CR-39($C_{12}H_{18}O_7$) detectors are studied. The experimental results are compared with the predictions of the theoretical models and other experimental results at different beam energies.

2 Experimental setup

Stacks of C, Al and CH_2 targets sandwiched with CR-39 detectors (HARZLAS TD-1) were exposed normally to 400 A MeV ^{20}Ne beams at the Heavy Ion Medical Accelerator in Chiba (HIMAC) at the Japanese National Institute of Radiological Sciences

Received 2 April 2011

* Supported by National Natural Science Foundation of China (11075100, 10975019), Shanxi Provincial Foundation for Returned Overseas Chinese Scholars, China (2011-058), Natural Science Foundation of Shanxi Province, China (2011011001-2), and Scientific Research Foundation for Returned Overseas Chinese Scholars, Ministry of Personnel (MOP2006138)

1) E-mail: zhangdh@dns.sxnu.edu.cn

(NIRS). The beam density is about 2000 ions/cm^2. The configuration of the sandwiched target is shown in Fig. 1. A CR-39 sheet, about 0.77 mm in thickness, is placed before and after the targets. The thicknesses of the carbon, aluminum and polyethylene targets are 5, 3 and 10 mm, respectively.

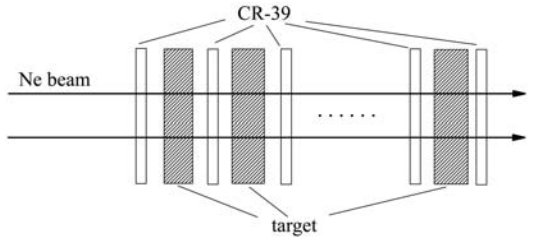

Fig. 1. Sketch of the target-detector configuration.

The CR-39 detectors are etched in 3M NaOH aqueous solution at 70 ℃ for 15 h. Then, the beam ions and their fragments manifest in the CR-39 as etch-pit cones on both sides of the detector. The base areas of the etch-pit cones (tracks) are automatically measured and analyzed using the HSP-1000 microscope system and PitFit track measurement software. Image data (45 mm×45 mm area) are acquired for both the front and back surfaces of each detector. 2×10^4 ^{20}Ne ions are traced from the first detector surface in the stack.

3 Data collection

The trajectories of ion tracks through CR-39 sheets are reconstructed in two steps: (1) the track position in CR-39 is corrected by parallel and rotational translation of coordinates (x and y) of tracks formed in the detectors, and (2) the difference between the position of the corresponding tracks on the surfaces in the neighboring detector is minimized by a track matching routine.

The coordinate (x and y) of tracks formed in the detectors is translated because of microscope scanning technology. The coordinate of tracks before the target (or front surface) is (x, y) and of matching tracks after the target (or back surface) is (x', y'). Following the translation relation, the coordinate of matching track can be calculated as:

$$x'_{\rm cal} = ax+by+c, \tag{1}$$

$$y'_{\rm cal} = a'x+b'y+c', \tag{2}$$

parameters a, b, c, a', b' and c' are fitted using the least square methods. The coordinate $x'_{\rm cal}$, $y'_{\rm cal}$ of the matching track is calculated. Certainly, $x'_{\rm cal}$, $y'_{\rm cal}$ are different from x', y', and the difference $\mathrm{d}x = x'_{\rm cal} - x'$, $\mathrm{d}y = y'_{\rm cal} - y'$ is calculated, which can help us to determine the matching track.

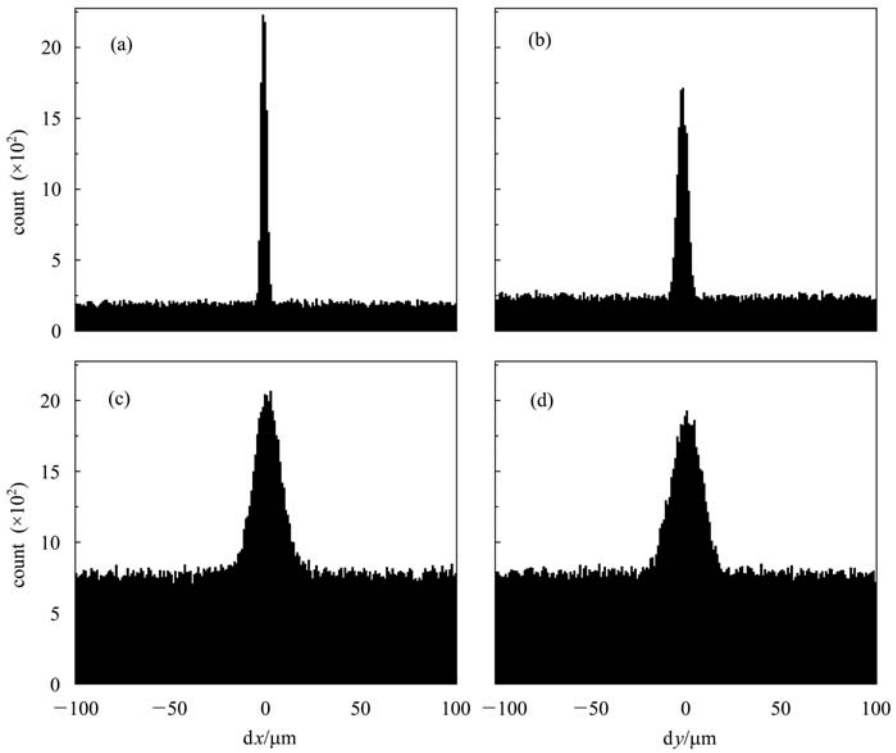

Fig. 2. The differences (dx and dy) for x and y given by the subtraction of track coordinates on the other surface. (a) and (b) are the differences between the front surface and the back surface on a detector, and (c) and (d) are the differences before and after the Al target.

Figure 2(a) and (b) show the track position difference in the front surface and back surface on a CR-39 sheet, Fig. 2(c) and (d) show the track position difference before and after the target. If the differences are calculated for all combinations of positions for extracted tracks, only the matching combination ought to make a peak which appears in the figures, and the dx and dy values of the other combinations should be randomly distributed. The deviations ($\sigma(x)$ and $\sigma(y)$) give the position accuracies of the tracks, which are estimated to be 2–5 μm between the front and back surface of one detector and 15–40 μm before and after the targets. The accuracy suffers from Coulomb scattering with energy loss straggling and becomes significant on the downstream detectors. However, since $\sigma(x)$ and $\sigma(y)$ take the maximum value in our investigation, the overall effect is negligible.

Both the front and back surfaces are measured automatically by PitFit software and then checked manually. The trajectory of Ne ions passing through the detectors is determined by searching for the tracks on each surface within $\pm 4\sigma(x)$ and $\pm 4\sigma(y)$ distances of x and y for the top detector surface [18]. There are two cases, with or without candidate track, when matching the tracks on adjacent detector surfaces. The latter is a candidate event for fragmentation reaction. The former can be divided into three further cases: 1) if the area of the track is smaller than that of the beam track, we consider it a candidate event for fragmentation reaction; 2) if the area of the track is equal to that of the beam track, we consider it without any nuclear reactions; and 3) if the area is larger than that of the beam track, then it is regarded as a charge pick-up reaction.

3.1 Total charge-changing cross sections

The base area distributions in the CR-39 sheet of Ne ions and produced fragments (on the CH_2 target) are shown in Fig. 3. Gaussian fittings are made in each peak and the charge of projectile fragment is identified by the base area distribution. The maximum value of Ne ion base distribution is 450.6 μm^2, which is about 499 counts.

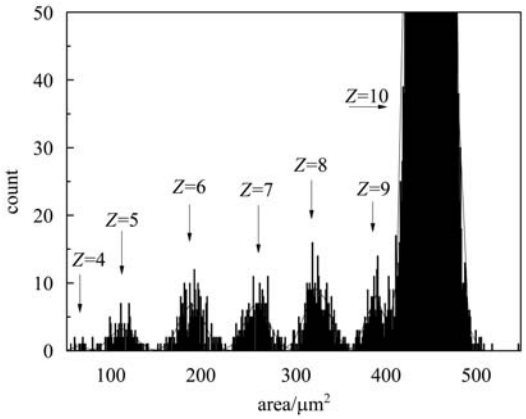

Fig. 3. The base area distribution of Ne ions and their fragments in CR-39. Gaussian fits are made in each peak.

The total charge-changing cross sections are determined by the relation [15]

$$\sigma_{\rm tot} = \frac{A_{\rm T} \ln(N_{\rm in}/N_{\rm out})}{\rho_{\rm T} D N_{\rm AV}}, \tag{3}$$

where $A_{\rm T}$ is the nuclear mass of the target. $N_{\rm in}$ and $N_{\rm out}$ are the numbers of beam ions before and after the target, respectively, $\rho_{\rm T}$ is the target density, D is the thickness of the target and $N_{\rm AV}$ is the Avogadro number. The cross section for the H target is deduced from the measured cross sections of CH_2 and the C target as:

$$\sigma_{\rm H} = 0.5(\sigma_{\rm CH_2} - \sigma_{\rm C}). \tag{4}$$

Table 1 shows the results of the total experimental charge-changing cross sections of ^{20}Ne on the H, C, Al and CH_2 targets. For comparison, the data with various theoretical models and other experimental results [7, 9, 19, 20] are also listed in the table. We also use the Bradt-Peters semi-empirical formula [21] $\sigma_{\rm tot} = \pi r_0^2 (A_{\rm P}^{1/3} + A_{\rm T}^{1/3} - b_0)^2$ to calculate the total charge-changing cross sections, where $A_{\rm P}$ and $A_{\rm T}$ are the projectile and target mass numbers, $r_0 = 1.35$ fm and $b_0 = 0.83$. The Bradt-Peters formula cannot be directly used in the case with a hydrogen target because of the so-called overlap parameter b_0 and the scaled nucleus radius $r_0 A^{1/3}$. We choose $A_{\rm T} = 0.089$ [22] to calculate the total charge-changing cross section for ^{20}Ne on the H target. It is found that the results from the Bradt-Peters formula are in agreement with our experimental results. Predictions from NUCFRG2 and PHITS are also reasonably in agreement with the experimental results, except for the Al target result. Finally, our results are consistent with the other ones at the investigated energies [7, 9, 19, 20].

3.2 Partial charge-changing cross sections

The partial fragmentation cross sections of the fragment with charge Z can be calculated using the relation [15]

$$\sigma_Z = \frac{A_{\rm T}}{\rho_{\rm T} D N_{\rm AV}} \left(\frac{N_{\rm out}^{\rm f}}{N_{\rm out}^{\rm p}} - \frac{N_{\rm in}^{\rm f}}{N_{\rm in}^{\rm p}} \right), \tag{5}$$

where $N_{\rm in}^{\rm f}$ and $N_{\rm out}^{\rm f}$ are the numbers of fragments with charge Z before and after the target.

Table 1. The total experimental charge-changing cross sections (in mb) for interactions of ^{20}Ne with H, C, Al and CH_2 targets, and the predictions from different models.

	H	C	Al	CH_2
present work	308±11	1024±24	1406±41	1642±35
Bradt-Peters	311	997	1365	
400 *A* MeV, NUCFRG2 [7]	298	1078	1481	
400 *A* MeV, PHITS [7]	305	983	1416	
600 *A* MeV, Ref. [19]	299±9	987±29	1354±41	
540 *A* MeV, Ref. [20]	298±6	951±10		1550±16
645 *A* MeV, Ref. [20]	319±6	980±10		1619±16
670 *A* MeV, Ref. [20]	378±7	977±10		1621±16
1096 *A* MeV, Ref. [20]	330±7	998±10		1662±16
100 *A* MeV, Ref. [9]		1161±80	1446±120	
200 *A* MeV, Ref. [9]		1123±80		
300 *A* MeV, Ref. [9]		1168±100	1328±120	
290 *A* MeV, Ref. [7]	272±16	1050±21	1445±45	
400 *A* MeV, Ref. [7]	311±15	1034±21	1438±26	
600 *A* MeV, Ref. [7]	319±13	986±14	1349±30	

Table 2. The partial cross sections (in mb) for fragment production in interactions of ^{20}Ne on H, C, Al and CH_2 targets.

beam and target	$Z_{\rm frag}=9$	$Z_{\rm frag}=8$	$Z_{\rm frag}=7$	$Z_{\rm frag}=6$	$Z_{\rm frag}=5$
present work, H target	52±4	73±5	57±5	40±4	35±4
present work, C target	72±9	136±13	112±11	119±12	50±7
present work, Al target	97±17	166±22	134±20	149±21	34±10
present work, CH_2 target	174±17	282±22	224±20	119±19	111±14
600 *A* MeV, H target [19]	52±4	71±6	52±5	54±5	22±4
600 *A* MeV, C target [19]	83±4	132±6	101±4	124±5	66±3
600 *A* MeV, Al target [19]	115±5	159±7	123±6	151±7	78±4
290 *A* MeV, H target [7]	49±3	78±4	54±3	48±3	11±4
290 *A* MeV, C target [7]	109±3	163±4	128±4	161±4	75±5
290 *A* MeV, Al target [7]	130±5	188±7	155±6	190±7	100±4
400 *A* MeV, H target [7]	47±3	81±4	55±3	55±3	22±2
400 *A* MeV, C target [7]	102±3	151±4	117±3	144±4	79±4
400 *A* MeV, Al target [7]	120±3	178±5	144±4	170±5	98±5
600 *A* MeV, H target [7]	53±2	75±3	55±3	56±3	26±2
600 *A* MeV, C target [7]	84±2	134±3	101±2	124±3	65±2
600 *A* MeV, Al target [7]	106±3	158±5	123±4	152±5	81±3
540 *A* MeV, H target [23]	44.6±2.2	81.6±4.1	61.2±3.1	55.6±2.8	13.1±1.3
540 *A* MeV, C target [23]	106.3±1.6	181.0±2.7	134.5±4.0	135.1±4.1	63.7±2.7
645 *A* MeV, H target [23]	48.7±2.4	74.6±3.7	60.1±3.0	59.1±3.0	14.3±1.4
645 *A* MeV, C target [23]	91.6±1.4	150.6±2.3	111.1±3.3	125.9±3.8	52.6±2.6
670 *A* MeV, H target [23]	44.8±2.2	67.7±3.4	62.3±3.1	56.5±2.8	17.6±1.8
670 *A* MeV, C target [23]	96.9±1.5	159.5±2.4	118.8±3.6	120.2±3.6	53.6±2.7
1096 *A* MeV, H target [23]	47.1±2.4	73.6±3.8	56.7±2.8	62.4±3.1	22.1±2.2
1096 *A* MeV, C target [23]	87.6±1.3	140.1±2.1	103.0±3.1	119.8±3.6	57.2±2.9

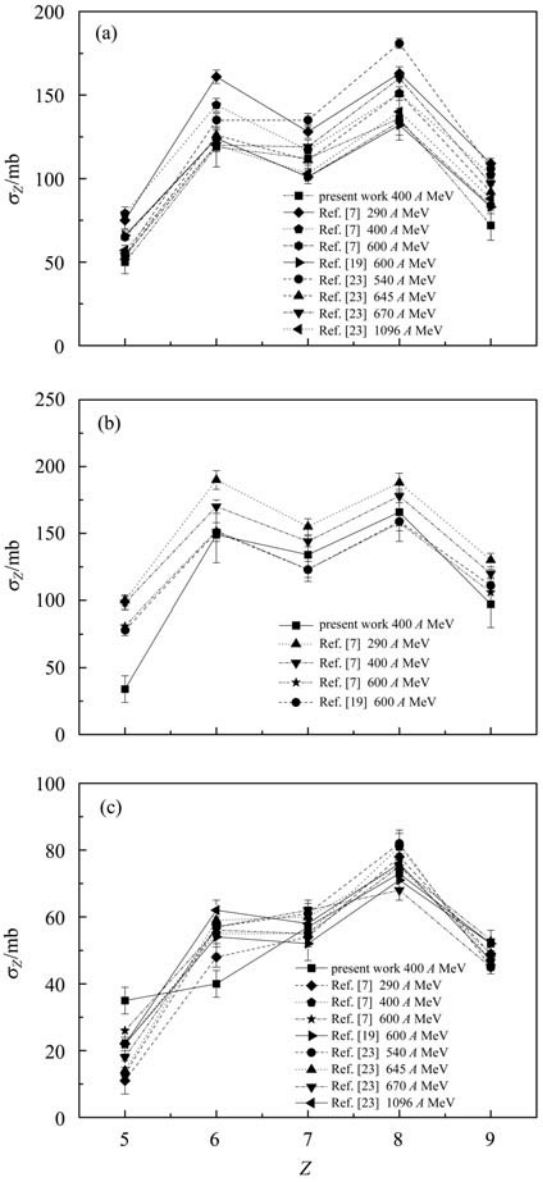

Fig. 4. The dependence of the partial cross section of fragment production on the charge of fragment in collisions of ^{20}Ne with C (a), Al (b) and H (c) targets.

Because Ne ion tracks are only measured before the targets, $N_{\rm in}^{\rm f}=0$. In this case, Eq. (5) can be simplified as

$$\sigma_Z=\frac{A_{\rm T}}{\rho_{\rm T}tN_{\rm AV}}\frac{N_{\rm out}^{\rm f}}{N_{\rm out}^{\rm p}}. \qquad (6)$$

The partial cross sections for projectile fragment production in interactions of 400 A MeV ^{20}Ne on H, C and Al targets are presented in Table 2. Compared with the results reported in other experiments [7, 19, 23], we can see that our results are slightly smaller than the other results at the same energy.

Figure 4 shows the variation of the partial cross sections with the charge of projectile fragments for the interactions of ^{20}Ne with the H, C and Al targets, respectively. An obvious odd-even effect is observed in the projectile fragment production in all interactions. The odd-even effect can be quantitatively studied by the quantity $V(Z_{\rm f})$, defined as [11]

$$V(Z_{\rm f})=2\sigma(Z_{\rm f})/[\sigma(Z_{\rm f}+1)+\sigma(Z_{\rm f}-1)], \qquad (7)$$

where $Z_{\rm f}$ refers to the fragment of charge Z. We combine the values of $V(Z_{\rm f})$ obtained for all odd-Z fragments into a single weighted-average value, and similarly combine the results for all even-Z fragments to get that weighted average, and take the ratio of the two to obtain a single value for a given beam ion and energy. For 400 A MeV ^{20}Ne beams, we can calculate $V(Z_{\rm f})$ only for the fragments with charges of 6, 7 and 8. We find that the ratio for our experimental results is 1.55±0.02, which is close to the result (1.73±0.04) [7] at the same beam energy.

4 Conclusions

The total charge-changing cross sections and partial cross sections for the fragment production of 400 A MeV ^{20}Ne ions in collision on H, C, Al and CH_2 targets are investigated. The experimental results are compared with various theoretical models and other experimental results at different energies. It is found that our experimental results of total charge-changing cross sections are consistent with the other experimental results at the same and nearly the same beam energies, and the predictions from the theoretical models. Finally, the partial cross sections for fragment production are smaller than the other experimental results at the same and nearly the same energies, and the odd-even effect is clearly observed in our data sets.

References

1 CHEN C X, Albergo S, Caccia Z et al. Phys. Rev. C, 1994, **49**: 3200–3210
2 Petti P L, Lennox A J. Annu. Rev. Nucl. Part. Sci., 1994, **44**: 155–197
3 Lynch W G. Ann. Rev. Nucl. Part. Sci., 1987, **37**: 493–535
4 Townsend L W, Ramsey C R, Tripathi R K et al. Nucl. Instrum. Methods B, 1999, **149**: 401–413
5 Botvina A S, Mishustin A S. Eur. Phys. J. A, 2006, **30**: 121–128
6 Mocko M, Tsang M B, Lacroix D et al. Phys. Rev. C, 2008, **78**: 024612
7 Zeitlin C, Miller J, Guetersloh S et al. E-print, arXiv: 1102.2848vl, [Nucl-ex], Feb.14, 2011
8 Schall I, Schardt D, Geissel H et al. Nucl. Instrum. Methods B, 2008, **117**: 221–234
9 Kox S, Gamp A, Perrin C et al. Phys. Rev. C, 1987, **35**: 1678–1691
10 Cummings J R, Binns W R, Garrard Y L et al. Phys. Rev. C, 1990, **42**: 2508–2529
11 Iancu G, Flesch F, Heinrich W. Radiat. Meas., 2005, **39**: 525–533
12 Zeitlin C, Fukumura A, Guetersloh S B et al. Nucl. Phys. A, 2007, **784**: 341–367
13 Nilsen B S, Waddington C J, Cummings J R et al. Phys. Rev. C, 1995, **52**: 3277–3290
14 Toshito T, Kodama K, Sihver L et al. Phys. Rev. C, 2008, **75**: 054606
15 Cecchini S, Chiarusi T, Giacomelli G et al. Nucl. Phys. A, 2008, **807**: 206–213
16 Amaldi U. Nucl. Phys. A, 2005, **751**: 409–428
17 Wilson J W, Thibeault S A, Cucinotta F A et al. Radiat Environ Biophys, 1995, **34**: 217–222
18 Ota S, Kodaira S, Yasuda N, Benton E R et al. Radiat. Meas., 2008, **43**: S195–S198
19 Zeitlin C, Fukumura A, Heibronn L et al. Phys. Rev. C, 2001, **64**: 024902
20 Webber W R, Kish J C, Schrier D A. Phys. Rev. C, 1990, **41**: 520–532
21 Bradt H C, Peters B. Phys. Rev., 1950, **77**: 54–70
22 Westfall G D, Wilson L W, Lindstrom P J et al. Phys. Rev. C, 1979, **19**: 1309–1323
23 Webber W R, Kish J C, Schrier D A. Phys. Rev. C, 1990, **41**: 533–546